Radiation damage production in massive cascades initiated by fusion neutrons in tungsten

A. E. Sand[a,*], K. Nordlund[a], S. L. Dudarev[b]

[a]*EURATOM-Tekes, Department of Physics, P.O. Box 43, FI-00014 University of Helsinki, Finland*
[b]*EURATOM/UKAEA Fusion Association, Culham Centre for Fusion Energy, UK*

Abstract

Neutrons in fusion reactors produce primary radiation damage from displacement cascades in tungsten (W) at an average PKA energy of 150 keV. We find, using molecular dynamics simulations, that cascades at this energy do not break up into subcascades. The massive amount of energy concentrated in the liquid-like heat spike facilitates a fairly high rate of formation of large dislocation loops and other defect structures, of sizes readily visible in today's electron microscopes. We investigate the structures and distribution of the cascade debris in W predicted by different interatomic potentials. In particular, our simulations show the formation of $\langle 100 \rangle$ -type dislocation loops, in agreement with recent experiments and in contradiction to the earlier held view that only $1/2\langle 111 \rangle$ -type loops occur in W.

Keywords:
tungsten, radiation damage, collision cascades, molecular dynamics

1. Introduction

Tungsten (W), with its unique combination of properties including good thermal conductivity and high melting point, combined with resistance to erosion and low neutron activation, is a candidate material for both structural and plasma-facing components in current and future fusion reactors. However, the brittleness of tungsten poses a problem, and in addition little is currently known on the radiation embrittlement from the long-term effects of high neutron doses. The precise nature of defect structures formed in cascades constitutes a key factor determining microstructural evolution of the material, and is crucial for predicting the performance of components during the lifetime of the reactor.

The high-energy neutrons produced by the D-T fusion plasma [1] give rise to primary recoils in tungsten with average energies of around 150 keV. Recent *in situ* TEM observations [2] of 150 keV self-ion irradiated W have shown

---

*Corresponding author
Email address:* `andrea.meinander@helsinki.fi` (A. E. Sand)

the occurrence of novel cascade damage from single ion impacts. These experiments offer a unique opportunity for direct comparison of cascade simulations to experiment. For this purpose we have performed molecular dynamics (MD) simulations of 150 keV collision cascades in W, comparing the predictions of different interatomic potentials.

Cascade damage has been extensively studied by MD methods, and in particular, it has been shown that damage production becomes a linear function of recoil energy after the onset of subcascade break-up [3]. However, cascade damage in W has previously been studied by MD methods for energies only up to 100 keV [4]. The simulations described in this work show that even at 150 keV, break-up is not complete. The high energy density in the compact cascades gives rise to collective effects which have a significant effect on damage production. The precise nature of defect structures provides input for models aimed towards predicting defect evolution in tungsten.

There are still large uncertainties considering the numbers of defects produced in W. The SRIM recommended value for the threshold displacement energy (TDE) used in the NRT model is $E_d = 90$ eV, whereas experiment [5] gives a lower TDE, suggesting that the rate of defect production should be higher than what the SRIM/NRT model predicts. This is unusual, for example cascade simulations in iron predict defect numbers significantly lower than the NRT model. The full MD simulations of cascades in W performed in this work cast light on this issue.

2. Methods and analysis

MD simulations of collision cascades from 150 keV recoils have been performed using the PARCAS code [6]. Simulations were performed at 0 K to include only athermal processes in defect creation. Cubic simulation cells with periodic boundaries, of 48 nm to a side and containing over 6 million atoms, were used for each cascade. A Berendsen thermostat [7] was applied to cell borders, and each cascade was simulated for 40 ps, at which point the cell had cooled to an average temperature of only a few K.

Three different potentials were compared. Most simulations were done using the modified EAM potential by Derlet *et al.* [8] (hereafter denoted by D-D), with the repulsive part given by the universal Ziegler-Biersack-Littmark potential [9], fitted by Björkas *et al.* [10]. These were compared to simulations using Ackland-Thetford EAM potential (A-T) [11], and a more recent Tersoff-type potential by Ahlgren *et al.* (A-H) [12]. The predicted TDE for the latter two potentials was determined by the method described in Ref. [13]. Simulation cells with 38400 atoms, initially with half liquid and half crystal structure, were used to find the melting points for the D-D and A-T potentials.

The simulations incorporate electronic energy losses in the form of electronic stopping (ES) given by SRIM [14]. This is implemented as a friction term, and requires the use of a lower energy threshold T_c, below which the friction term is not applied, else all thermal modes are quickly quenched. To check the effect

of this, the value of T_c was varied from 1 eV to 100 eV in simulations using the D-D potential.

Defects were detected with two methods which were then compared to each other and found to agree completely. On the one hand atoms were filtered according to potential energy, and those with 0.2 eV higher than the potential's predicted cohesive energy were singled out. This was compared to defects identified using an automated Wigner-Seitz cell method [15].

Large irregular defect structures were relaxed separately at 600 K for 100 ps.

The size and shape of a cascade was determined by analysing the liquid atoms at the time the liquid-like area was largest, approximately after the first 300 fs. An atom was determined to be liquid when the average energy of the atom and its neighbors exceeded the energy corresponding to the melting temperature.

3. Results and discussion

3.1. Defect numbers

Collective effects occurring in the cascade heat spike, such as recombination, play an important role in defect production. Although thermally activated recombination is not included in these simulations, nevertheless the number N_{FP} of surviving defects is far less than the number N_{NRT} predicted by the NRT model [16].

N_{NRT} is a function of damage energy T_d, i.e. the amount of energy which has gone to the ionic system. In these simulations, T_d is given by the initial PKA energy minus the energy which is removed from the system as a result of electronic stopping. In cascades simulated with the D-D potential and $T_c = 10$ eV, $T_d \approx 110$ keV (see Table 1), and the efficiency, calculated as N_{FP}/N_{NRT}, is 0.4. The same efficiency is predicted when $T_c = 1$ eV, with lower defect numbers balancing the lower T_d, while $T_c = 100$ eV gives an efficiency of 0.5. The direction-specific TDEs predicted by the D-D potential agree very closely with the experimental values, while the average over all directions is very close to the higher NRT value [10], since E_d is higher in higher index directions. These simulations are thus consistent with both the experimental TDE and the NRT recommended E_d value.

The TDE predicted by the A-H potential is also in reasonable agreement with experiment, with $E_d = 39 \pm 1$, 69 ± 1 and 89 ± 1 in the $\langle 100 \rangle$, $\langle 110 \rangle$ and $\langle 111 \rangle$ directions, respectively. However, the efficiency predicted by cascade simulations is only 0.2. With the A-T potential the efficiency is 0.3, although the predicted TDE is higher ($E_d = 57 \pm 1$, 103 ± 1 and 41 ± 1 in the $\langle 100 \rangle$, $\langle 110 \rangle$ and $\langle 111 \rangle$ directions, respectively). The efficiency is thus sensitive to the potential for other reasons than the predicted TDE.

Rather, N_{FP} is affected by the difference in cluster sizes appearing in the cascade debris. Simulations with the D-D potential give the largest SIA clusters, and correspondingly the highest average number of defects. This is due to the fact that large SIA clusters support large numbers of defects, while cascades with

3

T_d	N_{FP}	Cl_{max}^{vac}	Cl_{max}^{SIA}	F_{vac}	F_{SIA}	E_{ES} [keV]
1 eV	122.2 ± 2.9	5	54	0.00	0.47 ± 0.03	82.5 ± 1.2
5 eV	182.8 ± 27.9	118	164	0.21 ± 0.07	0.71 ± 0.07	47.6 ± 0.65
10 eV	179 ± 21.0	96	175	0.19 ± 0.06	0.72 ± 0.06	42.9 ± 0.6
20 eV	183 ± 18.1	72	94	0.16 ± 0.06	0.81 ± 0.01	39.1 ± 0.227
100 eV	257 ± 49.7	177	224	0.28 ± 0.10	0.81 ± 0.05	34.6 ± 1.55

Table 1: Defect numbers N_{FP}, the size of the largest vacancy (Cl_{max}^{vac}) and SIA cluster (Cl_{max}^{SIA}), and the fraction of vacancies (F_{vac}) and SIAs (F_{SIA}) in clusters larger the 4, for different ES cut-off energy T_c and using the D-D potential. The total energy E_{ES} lost to electronic stopping during the simulation is given in the last column.

only small clusters also have fewer defects in total. Although the Tersoff-type A-H potential tested in this work has lower TDEs than the other two potentials, it produces no large clusters, and has an average of only 90 Frenkel pairs per cascade. The A-T potential predicts roughly 30% fewer Frenkel pairs than the D-D potential, and accordingly the SIA clusters are slightly smaller.

3.2. Effects of the electronic stopping threshold

The time plot in Fig. 1 of the cumulative ES energy losses shows no difference during the first 250 fs for different T_c. This is the ballistic phase of the cascade, when recoils are very energetic, and the number of atoms with kinetic energy less than 100 eV is negligible. Thus the energy lost to ES is derived almost exclusively from atoms with energies above 100 eV. As a result, the use of a low-energy cut-off, and the choice of its value, does not affect the development of the cascade until the very end of the ballistic phase, when lower energy atoms begin to appear.

After the ballistic phase is over, during the thermal phase, the subsequent electronic energy losses for different T_c values above 5 eV are minimal, since most atoms at this point have energies below 5 eV. However, with $T_c = 1$ eV, a large amount of energy is still lost to the electronic system during the thermal phase, due to the large number of atoms in this phase that have energies just above 1 eV. The energy losses affect the formation of defect clusters, with only small clusters forming when $T_c = 1$ eV, and large clusters appearing when $T_c \geq 5$ eV (see Fig. 2).

3.3. Cascade morphology

The relatively short distance of propagation of even the highest-energy recoils in W, combined with the lower energy disturbance caused by their passage, results in a continuous liquid area which occasionally gives rise to large interstitial clusters. These are found around the perimeter of the liquid area, suggesting that they have formed by the liquid isolation mechanism [15]. The occurrence of very large SIA clusters is accompanied by a vacancy-rich core, often containing a large vacancy cluster, and in general the larger the SIA cluster is, the closer
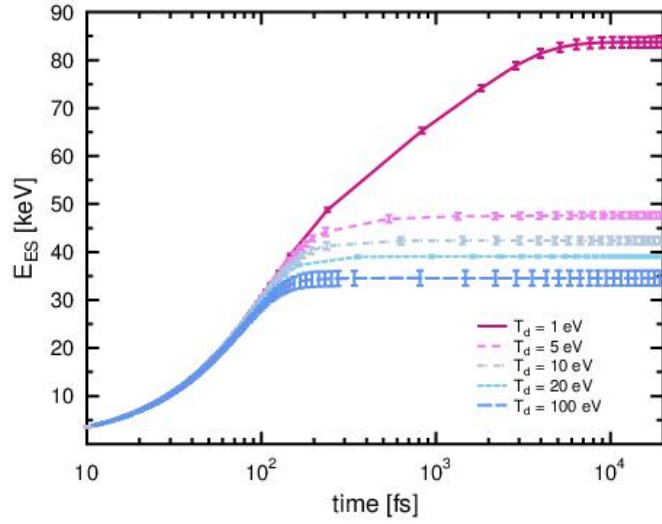
Figure 1: (Color online) Total cumulative electronic stopping E_{ES} in cascades with different T_c, using the D-D potential.
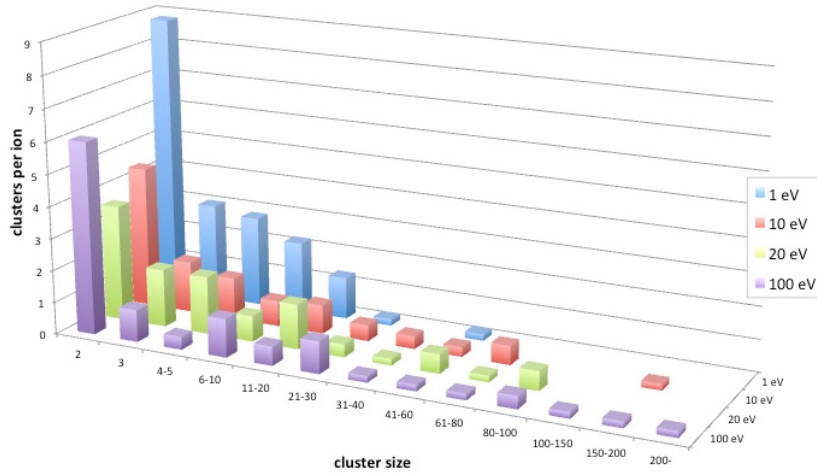
Figure 2: (Color online) Size distribution of defects for cascades simulated with the D-D potential, using different T_c.

it lies to the accompanying vacancy cluster. Large clusters appear in areas of cascades which are compact and almost spherical, which also take the longest to recrystallize. The maximum possible size of SIA clusters that can form at a given PKA energy is thus determined by the size of a compact cascade, rather than by the maximum extent of an elongated, partially split cascade. In many cascades where no large clusters have formed, the onset of cascade splitting can be inferred from the occurrence of a small number of SIAs between areas of vacancies, possibly evidence of collisions of pressure fronts as described by Calder *et al.*[17].

Simulations show that the size distribution of larger SIA clusters follows a power law $F(n) = 7.45n^{-1.63}$ [18]. This law is valid up to the size of the largest possible cluster formed in a cascade. The above power law also shows that the total average number of defects produced in a cascade equals $N = \sum_1^{n^*} nF(n) \approx 20.1 \cdot (n^*)^{0.37}$, where n^* is the size of the largest defect cluster. N is a monotonic function of n^*, suggesting that the occurrence (or non-occurrence) of cascade break up can be explored experimentally by investigating the dependence of the size of the largest defect cluster formed in a cascade as a function of the PKA energy.

3.4. Distributions and nature of defects

Approximately 60% of the cascades simulated with the D-D potential and $T_c \geq 10$ eV form large clusters. The debris from the remaining 40% resembles that from cascades with $T_c = 1$ eV, with only very small clusters, and the total average number of Frenkel pairs in these is only 120. Cascades which do produce large defect clusters retain a much higher total number of defects, while at the same time the number of isolated defects is relatively low. The large difference between these two cases means that an "average" cascade is not representative, and reasonable statistics requires the simulation of a large number of cascades.

When large clusters do form, SIA-type dislocation loops with both **b**=⟨100⟩ and **b**=1/2⟨111⟩ Burgers vector are found, in addition to more complex structures. Loops with **b**=⟨100⟩ typically contain 40-60 SIAs, while larger loops have **b**=1/2⟨111⟩, and a number of the largest complex structures also relax to 1/2⟨111⟩ -type loops after annealing at 600 K. For SIA-type loops with **b**=1/2⟨111⟩, the habit plane normal is often pointing towards the central vacancy cluster, whereas loops with **b**=⟨100⟩ lie on a plane intercepting the vacancy cluster. Mostly **b** is aligned in a direction which does not intercept the vacancy-rich core, and is thus not normal to the loop habit plane.

An example of the spacial distribution of defects is given in Fig. 3. A large, slightly distorted SIA-type dislocation loop consisting of 219 SIAs is visible in the foreground, close to the central vacancy cluster. The rest of the cascade debris spreads out towards the top right hand corner of the picture, and includes a small ⟨100⟩ SIA-type dislocation loop with 69 SIAs. The damage, which extends approximately 35 Å in the ⟨111⟩ direction, resulted from a recoil in the ⟨110⟩ direction.

Vacancy clusters exist mostly as under-dense areas of the lattice. Only one cascade, simulated with the A-T potential, collapsed into a large vacancy-type
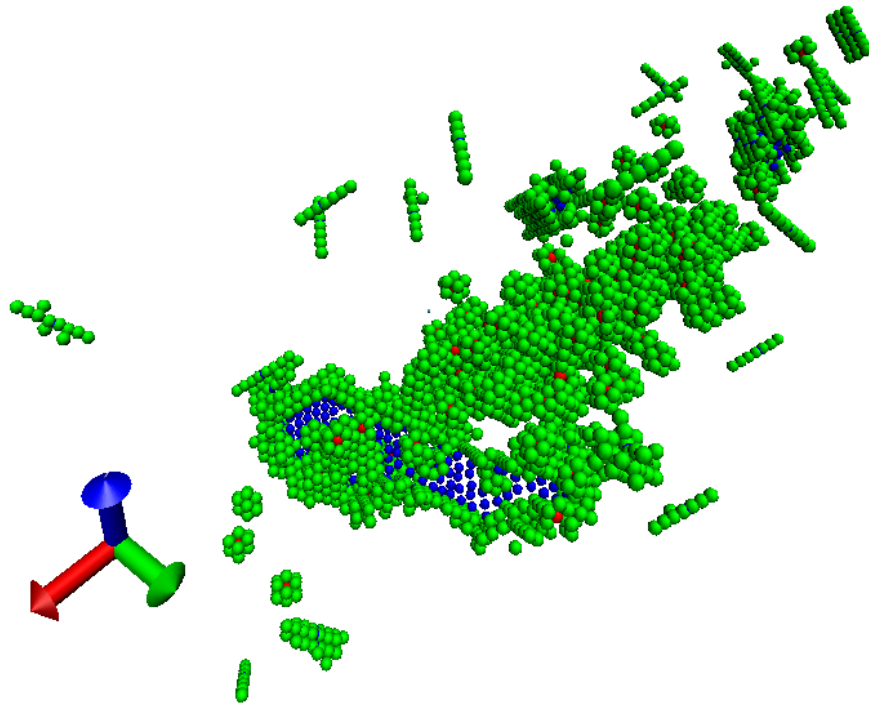
Figure 3: (Color online) The final damage configuration from a 150 keV PKA. Green spheres represent the W atoms with potential energy more than 0.2 eV higher than the cohesive energy. Blue spheres mark multiply occupied W-S cells, and red spheres indicate empty W-S cells.
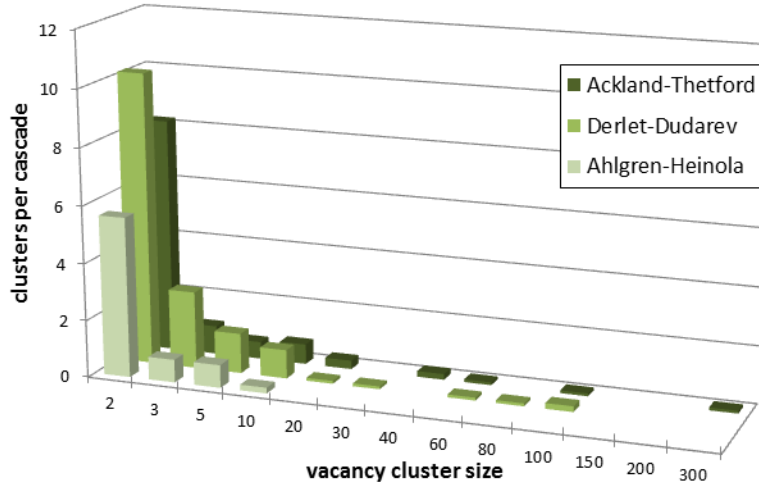
Figure 4: (Color online) The size distribution of vacancy clusters for cascades simulated in random directions, with the A-T, D-D and A-H potentials, using $T_d = 10$ eV.

loop consisting of 213 vacancies, with Burgers vector $\mathbf{b}=\langle 100 \rangle$. Cascade collapse is affected by the rate of cooling of the heat spike, with slower cooling increasing the probability of collapse [19]. The clustered vacancies observed with the D-D potential may therefore indicate cascades close to collapsing, which may collapse in higher temperature simulations.

Vacancy cluster sizes for the three potentials are shown in Fig. 4. The A-H potential produced no large vacancy clusters, probably due to the faster rate of recrystallization of the heat spike resulting from the high melting point predicted by the potential (4550 K [12]). A similar effect has been seen in Fe [20], and it is interesting to note that also in that case it was the Tersoff-type potential that failed to produce large clusters.

Vacancy clustering is also more affected than SIA clustering by the ES threshold, with no vacancy clusters forming with any potential when $T_c = 1$ eV, and the largest cluster seen when $T_c = 100$ eV. The energy removed from the heat spike during the thermal phase causes faster recrystallization of the liquid area, with the same effect on vacancy clustering as a higher melting point.

However, while simulations with A-T result in smaller SIA clusters than with D-D, and in total fewer Frenkel pairs, the fraction of vacancies in clusters is almost twice as high. This suggests that the rate of recrystallization of the heat spike is not the only mechanism affecting vacancy clustering, since the melting point predicted by D-D and A-T is practically the same, at $\tilde{3}900$ K and $\tilde{3}950$ K, respectively.

4. Conclusions

We find that cascades in W from 150 keV recoils do not to fully break up into subcascades. The resulting intense heat spike facilitates the athermal formation of large dislocation loops and other complex clusters from single cascades. The average number of Frenkel pairs formed in the cascades is strongly affected by the probability of large clusters forming among the debris, rather than by the predicted E_d of the potential. The efficiency of defect production compared to the NRT prediction thus depends on collective effects which arise in the heat spike, causing formation of large defect clusters, and is sensitive to the choice of interatomic potential.

The largest clusters of both SIA and vacancy type form where the cascade is the most compact. Based on the scaling law for SIA clusters, we suggest a method for experimentally investigating cascade break-up, using the relationship between the maximum cluster size for which the law is valid, and the total average number of defects produced in a cascade.

The choice of electronic stopping threshold in simulations also has a large effect on the clustering probability, by affecting the total electronic energy losses and thus the rate of cooling of the heat spike. The effect of T_c on vacancy clustering is especially pronounced, with rapid cooling of the heat spike when $T_c = 1$ eV completely inhibiting the formation of vacancy clusters. Since experiments indicate that large vacancy-type loops do form in single cascades, we conclude that $T_c = 1$ eV is too low for simulations of high-energy cascades, if an ES friction term alone is used to describe electronic energy losses.

Dislocation loops of both SIA and vacancy type with Burgers vectors $\mathbf{b}=\langle 100 \rangle$ and $\mathbf{b}=1/2\langle 111 \rangle$ occur in the cascade debris. This supports the interpretation of the recent *in situ* TEM experiments, where $\mathbf{b}=\langle 100 \rangle$ type loops in self-ion irradiated tungsten were reported.

[1] M. Gilbert, S. Dudarev, S. Zheng, L. Packer, J.-C. Sublet, Nuclear Fusion 52 (2012) 083019.

[2] X. Yi, M. L. Jenkins, M. B. no, S. G. Roberts, Z. Zhou, M. A. Kirk, Phil. Mag. A 93 (2013) 1715–1738.

[3] R. E. Stoller, G. R. Odette, B. D. Wirth, J. Nucl. Mater. 251 (1997) 49–60.

[4] M. J. Caturla, T. Diaz de la Rubia, M. Victoria, R. K. Corzine, M. R. James, G. A. Greene, J. Nucl. Mater. 296 (2001) 90–100.

[5] F. Maury, M. Biget, P. Vajda, A. Lucasson, P. Lucasson, Radiat. Eff. 38 (1978) 53–65.

[6] K. Nordlund, PARCAS computer code. The main principles of the molecular dynamics algorithms are presented in [21, 22]. The adaptive time step is the same as in [23], 2006.

[7] H. Berendsen, J. Postma, W. van Gunsteren, A. DiNola, J. Haak, The Journal of Chemical Physics 81 (1984) 3684–3690.

[8] P. M. Derlet, D. Nguyen-Manh, S. L. Dudarev, Phys. Rev. B 76 (2007) 054107.

[9] J. F. Ziegler, U. Littmark, J. P. Biersack, The stopping and range of ions in solids / J.F. Ziegler, J.P. Biersack, U. Littmark, Pergamon New York, 1985.

[10] C. Björkas, K. Nordlund, S. L. Dudarev, Nucl. Instr. Meth. B 267 (2009) 3204–3208.

[11] G. J. Ackland, R. Thetford, Phil. Mag. A 56 (1987) 15–30.

[12] T. Ahlgren, K. Heinola, N. Juslin, K. A., J. Appl. Phys. 107 (2010) 033516.

[13] K. Nordlund, J. Wallenius, L. Malerba, Nucl. Instr. and Meth. B 246 (2006) 322–332.

[14] J. F. Ziegler, SRIM-2008.04 software package, available online at *http://www.srim.org.*, 2008.

[15] K. Nordlund, R. S. Averback, Phys. Rev. B 56 (1997) 2421–2431.

[16] M. J. Norgett, M. T. Robinson, I. M. Torrens, Nucl. Eng. Des. 33 (1975) 50–54.

[17] A. Calder, D. Bacon, A. Barashev, Y. Osetsky, Philosophical Magazine 90 (2010) 863–884.

[18] A. E. Sand, S. L. Dudarev, K. Nordlund, EPL 103 (2013) 46003.

[19] C.A.English, M. Jenkins, Materials Science Forum 15-18 (1987) 1003–1022.

[20] C. Björkas, K. Nordlund, M. J. Caturla, Phys. Rev. B 85 (2012) 024105.

[21] K. Nordlund, M. Ghaly, R. S. Averback, M. Caturla, T. Diaz de la Rubia, J. Tarus, Phys. Rev. B 57 (1998) 7556–7570.

[22] M. Ghaly, K. Nordlund, R. S. Averback, Philosophical Magazine A 79 (1999) 795–820.

[23] K. Nordlund, Computational Materials Science 3 (1995) 448 – 456.